Journal of Materials Science: Materials in Electronics
https://doi.org/10.1007/s10854-019-02125-y

Variation in chemical bath pH and the corresponding precursor concentration for optimizing the optical, structural and morphological properties of ZnO thin films

Sunil Kumar[1] · H. C. Jeon[1] · T. W. Kang[1] · Rajni Seth[2] · Sanjay Panwar[3] · Surendra K. Shinde[4] · D. P. Waghmode[5] · Rijuta Ganesh Saratale[6] · Ravi Kant Choubey[7]

Received: 26 April 2019 / Accepted: 29 August 2019

Abstract

In the present study, ZnO thin films were deposited by chemical bath deposition carried out by selective correlation of varying (i) pH values at fixed concentration and (ii) concentration of the precursors at fixed pH. The selective correlations were done by using the characterization tools like X-ray diffraction, scanning electron microscopy, transmittance, refractive index, dielectric constant, Fourier-transform infrared spectroscopy and IV measurements. Transmittance was found to increase from 57 to 87% on varying the pH from basic side (10.8) to acidic side (pH 6.8) with a blue shift in band gap. The nature and morphology of the deposited films were found to be dependent on pH as well as concentration. Acidic pH 5.0 was found to be most suitable for deposition of highly transparent film with low absorption coefficient, refractive index and dielectric constant. On the other hand, nearly complete coverage of the substrate and high purity was observed in the ZnO thin films which was deposited by taking equal 100 mM concentration of $Zn(NO_3)$ and HMTA precursors at a fixed pH 5.0 as desired, sheet resistance was also found to increase on the acidic pH side which is useful in case of buffer layer solar cell application. These studies lay a foundation stone for understanding the optical and morphological parameters by selectively correlating the pH and concentration variation at the same time.

1 Introduction

Zinc oxide (ZnO) is a wide bandgap semiconducting material with unique chemical, optical and electrical properties. It has attracted considerable attention due to its various applications such as gas sensor [1], solar cell materials [2], antimicrobial materials [3, 4], optoelectronics devices [5, 6] and several other important applications [7]. These films are widely used as conductive and optical cover layers of large area solar cells [8, 9]. Different methodologies have been reported by several groups for deposition of ZnO nanostructures [10, 11]. Wet chemical techniques [12], physical vapor deposition [13], metal organic chemical vapor deposition (MOCVD) [14], pulsed laser deposition [15], molecular beam epitaxy (MBE) [16], sputtering [17], electrospinning [18] etc. are few common techniques. Most of these techniques are performed at high temperature and require expensive instrumentation. Wet chemical methods are comparatively simple, less expensive and reliable method.

Chemical bath deposition (CBD) is a low temperature wet chemical technique being widely used for the deposition of ZnO thin film buffer layers [19, 20]. It is a simple technique,

✉ Ravi Kant Choubey
ravikantchoubey@gmail.com

1 Nano Information Technology Academy, Dongguk University, Seoul 100715, South Korea

2 Department of Physics, Maharishi Markandeshwar University, Mullana, Ambala 133207, India

3 School of Basic and Applied Sciences, Maharaja Agrasen University, Baddi, Solan 174 103, India

4 Department of Biological and Environmental Science, College of Life Science and Biotechnology, Dongguk University, 32 Dongguk-ro, Biomedical Campus, Ilsandong-gu, Siksa-dong, Goyang-si, Gyeonggi-do 10326, South Korea

5 Department of Chemistry, Sadguru Gadage Maharaj College, Karad 415124, India

6 Research Institute of Biotechnology and Medical Converged Science, Dongguk University-Seoul, Ilsandong-gu, Goyang-si, Gyeonggi-do 10326, South Korea

7 Department of Applied Physics, Amity Institute of Applied Sciences (AIAS), Amity University, Noida Campus, Sector-125, Noida, U.P. 201 313, India

Published online: 03 September 2019

as morphological and structural properties of the grown films can be controlled by adjusting growth parameters such as pH, concentration, deposition time, bath temperature and choice of chelating agents [21, 22]. The important advantages of the CBD method are simplicity, low cost, low temperature, admirable large area uniformity and coverage [23–25]. In addition, many intrinsic defects which arise with high-temperature deposition techniques such as increased point defect concentrations, evaporation and decomposition of films [26] might also be avoided. Buffer layer deposition by CBD technique basically follows two mechanisms: (i) heterogeneous reaction and (ii) homogeneous reaction deposition [27]. Ion-by- ion deposition leads to heterogeneous reaction while cluster-by-cluster deposition occurred in homogeneous reaction. The homogeneous deposition leading to powdery and non-adherent films and hence is highly undesirable. Thin films deposited by such a process also feature scattering centers and peeling [28]. For a better quality films, the heterogeneous process is always desirable, in which adsorption of (Zn^{2+}) cation and anion (O^{2-}) takes place to form the thin films and yield better film quality.

From the extensive literature study, we observed that most of the ZnO thin films deposited by CBD are optimized by varying only one parameter out of pH, deposition time/temperature and precursor concentration independently. From best of our knowledge few scanty reports are available in which deposition of ZnO thin films have been studied by simultaneous optimization of parameters but nothing has been reported in which the parameters are selectively optimized leading to a best buffer layer ZnO sample. Hence, in the present study, attempts were made to deposit highly transparent and homogeneous ZnO thin films using CBD by selectively adjusting the pH as well as the concentration of chemical bath. These studies were performed with an objective to use the deposited thin films as an efficient buffer layer in thin film hetero-junction solar cell.

2 Experimental details

2.1 Deposition and growth of ZnO thin films

All the chemicals used were purchased by Sigma-Aldrich Company having purity level ≥ 99.0%. In order to study the effect of pH and precursor concentration on growth of ZnO thin films, two different sets of the deposited thin films were prepared. Zinc nitrate ($Zn(NO_3)_2{\cdot}6H_2O$) and hexamethylenetetramine (HMTA) have been used as precursors for the thin films fabrication by using a two-step chemical bath deposition process: coating of ZnO seeds on the cleaned glass substrate and further growth was carried out on the seeded substrate in an open bath maintained at a temperature of 90 °C. The substrates used were microscopic glass slides procured from Blue Cross India and cut into size of 2×2 cm^2. Before the deposition of the thin films, substrates were cleaned by dipping in chromic acid for 24 h. Thereafter, glass substrates were washed under running water, cleaned with detergent solution and further rinsed with water. Finally the glass substrates were rinsed with ethyl alcohol, acetone, Milli-Q water followed by ultra-sonication for 15 min. The glass substrates were then dried at 100 °C for 3 h. For deposition of seed layer on the cleaned glass substrate the procedure of Byrne et al. [29] was adopted. Dissolution of 25 mM of "zinc acetate dihydrate ($Zn(CH_3COO)_2{\cdot}2H_2O$)" was carried out in absolute ethanol (99%) followed by sonication for 15 min. Four micro litre (4 µL) of the above solution was put on the cleaned substrate by a micro syringe, followed by drying and then rinsing with distilled water. This process was repeated four times. In order to obtain thick dense seed layer, glass slides were further dipped in the above solution at 65 °C for 2 h in an oven, rinsed with distilled water and finally dried at 100 °C for 30 min.

The synthesis reaction was carried out in the aqueous medium. For CBD growth process, 100 mM of aqueous solutions of zinc nitrate hexahydrate "($Zn(NO_3)_2{\cdot}6H_2O$)" and hexamethylenetetramine "(HMTA)·($C_6H_{12}N_4$)" were prepared separately. The solutions were mixed together in equal ratio (1:1) and ultra-sonicated for 15 min. To study the effect of pH, the mixed solutions were adjusted to different pH as mentioned in Table 1 using concentrated nitric acid for preparing acidic bath and 1 N sodium hydroxide for basic bath and ultra-sonicated for 15 min. 50 ml solution mixture of the different pH was taken in four different glass beakers and four pretreated glass substrates were immersed in a slanting position. The beakers were maintained at 90 °C for 2 h in an oven. The samples were cooled, rinsed with distilled water and then air dried.

After deposition of ZnS thin films at various pH values and their subsequent characterizations, we deposited the thin films by varying the concentration of both the precursors but kept the ratio of the zinc salt and HMTA fixed every time as shown in Table 2. Also, during entire experiments the pH adjusted at "5.0" because we obtained satisfactory results on the films deposited at $pH_{5.0}$. The concentration variation studies were done to optimize the sample purity and the

Table 1 Growth conditions for deposition of ZnO thin films at various pH values

Sample code	100 mM $Zn(NO_3)_2$ (ml)	100 mM HMTA (ml)	pH	Deposition time (h)	Deposition Temp. (°C)
$pH_{6.8}$	50	50	6.8	2	90
$pH_{5.0}$	50	50	5.0	2	90
$pH_{10.8}$	50	50	10.8	2	90
$pH_{11.8}$	50	50	11.8	2	90

Table 2 Growth parameters for deposition of ZnO thin films at various concentrations

Sample code	$Zn(NO_3)$ Conc. (mM)	HMTA Conc. (mM)	pH	Deposition time (h)	Deposition Temp. (°C)
M_{25}	25	25	5.0	2	90
M_{50}	50	50	5.0	2	90
M_{75}	75	75	5.0	2	90
M_{100}	100	100	5.0	2	90

substrate coverage which is an important parameter for a making a final device.

The pH was adjusted using nitric acid and the solutions were adequately mixed using an ultra-sonication for 15 min. The seeded substrates were immersed into the solutions of above mentioned baths of different concentrations respectively and were kept at 90 °C for 2 h. The glass slides were finally rinsed with distilled water and dried in air. First of all, In order to examine the structural characteristics with respect to pH variation at fixed concentration, X-ray diffraction (XRD) patterns of all the samples were recorded by XPERT-PRO diffractometer (45 kV, 40 mA) which was equipped with a Goniometer PW3050/60 working with Cu Kα radiation of wavelength 1.5406 Å. Secondly, to study the effect of pH on the optical properties of deposited thin films, UV–VIS spectrophotometric studies were conducted in the wavelength range 250–800 nm using UV–VIS Spectrophotometer (Model UV-2550) with integrated sphere assembly ISR 240A with a resolution of 1 nm. Thirdly for studying both the effect of pH and precursor concentration, Fourier-transform infrared spectroscopy (FTIR) analysis was performed using Shimazdu IR Affinity-1S in the wavenumber range 0–4000 cm^{-1} and scanning electron microscope (SEM) HITACHI model S-3700N was used to observe the morphology of the particles in the thin films. Elemental phase compositions of deposited films were examined by energy dispersive X-ray spectroscopy (EDX). EDX system was integrated to the SEM where the electron beam excites characteristic X-rays from the probed area. Lastly, four probe electrical measurements using Keithley-2450 source meter (SMU) were done to find the resistivity (ρ) of the thin film for further calculating the sheet resistance (σ) using the thickness (t) and resistivity (ρ) values of the thin film in the following equation:

$$\rho = t\sigma \tag{1}$$

2.2 Reaction mechanism

$Zn(NO_3)_2{\cdot}6H_2O$ provided Zn^{2+} ions required for building up ZnO nano-structures, whereas HMTA ($(CH_2)_6N_4$) was used as a complexing agent. At natural pH, the presence of HMTA inhibited the rapid precipitation of zinc hydroxide and allowed a stable dispersion to be formed. It acted as a weak base and also as a buffer during the film deposition [30]. HMTA is non-ionic tetra-dentate cyclic tertiary amine with a high solubility in water, and gradually hydrolyzes in the aqueous solution at a slow rate to produce ammonia (NH_3) and formaldehyde HCHO under appropriate thermal conditions. NH_3 plays two important roles:

(i) It produces a basic environment by producing NH_4^+ and OH^- ions, which are necessary for the production of $Zn(OH)_2$. The chemical reactions can be summarized as follows.

Decomposition of HMTA:

$$\left(CH_2\right)_6N_4 + 6H_2O \rightarrow 6HCHO + 4NH_3 \tag{2}$$

Hydroxyl supply reaction:

$$NH_3 + H_2O \rightarrow NH_4OH \rightarrow NH_4^+ + OH^-$$

$$NH_3 + H_2O \rightarrow NH_4OH \rightarrow NH_4^+ + OH^- \tag{3}$$

Formation of $Zn(OH)_2$ reaction:

$$2OH^- + Zn^{2+} \rightarrow Zn(OH)_2 \tag{4}$$

Dehydration reaction leading to ZnO growth:

$$Zn(OH)_2 \rightarrow ZnO + H_2O \tag{5}$$

(ii) Secondly, it coordinates with the Zn^{2+} ions to produce zinc ammonia complex. Slow hydrolysis is important because if HMTA hydrolyzes rapidly and produces a large amount of OH^-, resulting in quick precipitation of Zn^{2+} ions in the solution due to high pH. As the reaction proceeds, Zn^{2+} ions are gradually consumed and decomposition of zinc-ammonia complex occurs slowly, resulting a very low level of super-saturation in the solution and thereby stabilize the concentration of Zn^{2+} ions. So, controlling the pH and concentration of Zn^{2+} ions promotes heterogeneous growth over homogeneous growth by avoiding a high ZnO saturation index. $Zn(OH)_2$ dehydrates into ZnO. The reaction mechanism can be summed up as [31].

$$Zn\left(NO_3\right)_2 \rightarrow Zn^{2+} + NO_3^- \tag{6}$$

$$C_6H_{12}N_4 + 10H_2O \rightarrow 6HCHO + 4NH_3H_2O \tag{7}$$

$$Zn^{2+} + 4NH_3H_2O \rightarrow \left[Zn\left(NH_3\right)_4\right]^{2+} + 4H_2O \tag{8}$$

$$\left[Zn\left(NH_3\right)_4\right]^{2+} + 4H_2O \rightarrow Zn(OH)_2 + 4\left[NH_4\right]^{2+} + 2OH^- \tag{9}$$

$$Zn(OH)_2 \rightarrow ZnO + H_2O \tag{10}$$

During the precipitation process, the formation of a solid phase should start in the solution when ionic product (I_p) exceeds the solubility product (k_{ps}) which depends upon the pH of the solution [32]. Since the solubility product for Zn $(OH)_2$ is 10^{-17}, under basic pH 10.8 due to higher reaction rate, Zn $(OH)_2$ precipitates very fast. This resulted in comparatively thicker films with less transmittance. Tada [33] reported that hydrolytic decomposition of protonated hexamine $[(CH_2)_6N_4H]^+$ takes place under acidic conditions, thereby producing protonated ammonia through the following reaction in the chemical bath:

$$\left[(CH_2)_6N_4\right] + H^+ \rightarrow \left[(CH_2)_6N_4H\right]^+ \tag{11}$$

$$\left[(CH_2)_6N_4H\right]^+ + 3H^+ + 4NO_3^- + 6H_2O \rightarrow 4NO_3^- + 6CH_2 \tag{12}$$

Under weak acidic conditions, ammonia combines with Zn^{2+} ions and produces enormous number of zinc–amino complexes in the solution. These complexes will be hydrolyzed directly to form ZnO on the glass substrate and on the inner surface of the vessel through the decomposition reaction. Hence, ammonia could stabilize Zn^{2+} ions through reversible reaction of consuming and decomposing of zinc–ammonia complex. It was observed that in acidic bath (pH 5.0), the solution remained transparent during deposition indicating a slow chemical deposition process. As a result thin films deposited at this pH exhibited higher transmittance.

3 Results and discussion

3.1 Thickness of thin films

Thicknesses of the thin films of ZnO deposited at various pH were calculated according to thermo-gravimetric method as described by Vijayan et al. [34] using the relation given below.

$$t = \frac{m}{A\rho} \tag{13}$$

where t is the thickness of the film, m is the weight gain, A is the area of the deposited film, ρ is the density of the film which was taken as 5.606 g/cm^3. The calculated values of thicknesses of samples $pH_{6.8}$, $pH_{5.0}$ and $pH_{10.8}$ were found to be 1.11 µm, 802 nm and 2.14 µm respectively. The last sample i.e. $pH_{11.8}$ showed visibly white and rough film with lot of pin holes with a thickness of 4.06 µm

3.2 Structural properties

The XRD patterns of the deposited films at different pH values are shown in Fig. 1a–c. X-ray diffraction spectrum for sample $pH_{6.8}$ manifests the presence of more than one phase. ZnO peaks correspond to the direction [100], [002] and [101], together with other supplementary peaks. These supplementary peaks in XRD spectra can be attributed to the presence of $Zn(OH)_2$ and silica in the substrate, which are further confirmed by FTIR studies. XRD spectra revealed the presence of wurtzite ZnO structure with prominent peak at 34.602° corresponding to [002] reflection, thereby confirming the polycrystalline nature of the films with preferred ***c***-axis orientation. XRD pattern of $pH_{5.0}$ for ZnO thin film at acidic pH (Fig. 1b) was found to be amorphous. Sample $pH_{10.8}$ exhibited polycrystalline wurtzite structure of ZnO (JCPDS data-card No. 36-1451). The shift in the positions of [100], [002] and [101] reflections in XRD spectra of $pH_{10.8}$ as compared to $pH_{6.8}$ is attributed to decrease in bond lengths [35]. With the increase in pH, the OH^- ions increased and suppressed the growth of ZnO nano-crystallites along the [002] axis (Fig. 1c) [36].

The lattice parameters "a" and "c" of wurtzite structure ZnO were calculated, according to well-known Bragg's law

$$2d \sin\theta = n\lambda \tag{14}$$

For hexagonal structure the relation between interplanar spacing "d" and lattice constants a and c is given by;

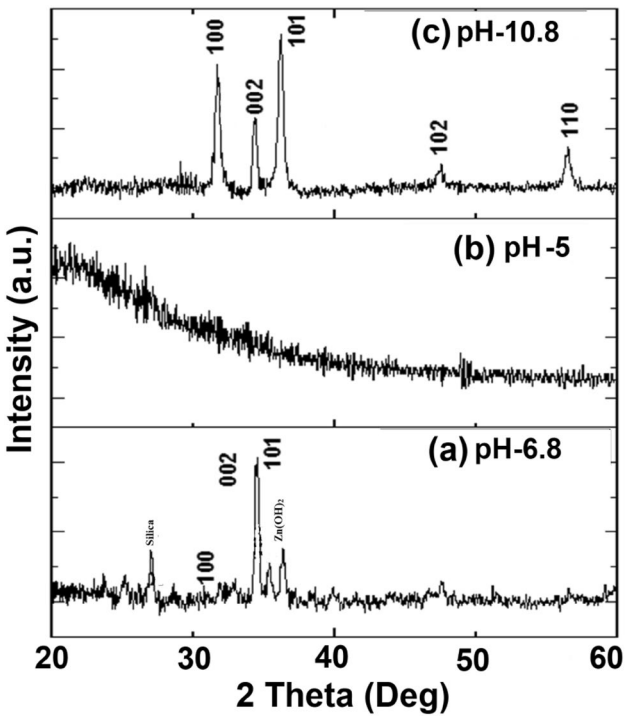

Fig. 1 XRD patterns of as deposited ZnO thin films at different pH values

$$\frac{1}{d_{hkl}^2} = \frac{4}{3}\left(\frac{h^2 + hk + k^2}{a^2}\right) + \frac{l^2}{c^2} \tag{15}$$

The lattice constants "a" and "c" of the nanocrystalline ZnO film deposited at $pH_{10.8}$ were calculated using the following relations

For (100) plane

$$a = \frac{\lambda}{\sqrt{3}\sin\theta} \tag{16}$$

For (002) plane

$$c = \frac{\lambda}{\sin\theta} \tag{17}$$

The diffraction planes and respective d-spacing values are tabulated in Table 3.

From above table it is clear that the calculated d-spacing values are in good agreement with the reported standard results [37]. Crystallite size for the samples $pH_{6.8}$ and $pH_{10.8}$ were determined by the well-known Scherrer's formula. It was found to be 8.19 ± 0.02 nm and 12.26 ± 0.02 nm for $pH_{6.8}$ and $pH_{10.8}$ samples, respectively. XRD spectra of sample $pH_{5.0}$ exhibited the amorphous nature of this sample (Fig. 1b) and indicated a shift in band edge. Short range grain size calculated using Brus equation [38] for $pH_{5.0}$ was found to be quite small (1.81 nm).

3.3 Optical properties

3.3.1 UV–Vis absorption spectroscopy

It is manifested that pH of the chemical bath affects the transmittance of ZnO thin films. Figure 2 exhibits the transmittance curves for all the four specimens prepared at different pH values. Transmittance of the thin film prepared at the natural $pH_{6.8}$ was found to be 78% with an absorption edge around 370 nm. However, in case of the sample $pH_{5.0}$, the transmittance increased up to 87%. Also, the blue shift in absorption edge was observed in comparison to $pH_{6.8}$. The film deposited at $pH_{10.8}$ shows tremendous decrease in transmittance to a level of 57% while the last sample $pH_{11.8}$ showed very poor transmittance therefore, not considered for further characterization. The fluctuations appeared on the transmittance spectra of this sample ($pH_{11.8}$) are due to the interference of light reflected between the air-film and film-glass interfaces [39].

Table 3 Calculated d-spacing value for $pH_{10.8}$ deposited ZnO thin films

Sample	(hkl)	2θ	d-spacing (Å)	
			Calculated	Standard
$pH_{10.8}$	(100)	31.66°	2.826	2.81
	(002)	34.30°	2.611	2.60
	(101)	36.23°	2.434	2.47

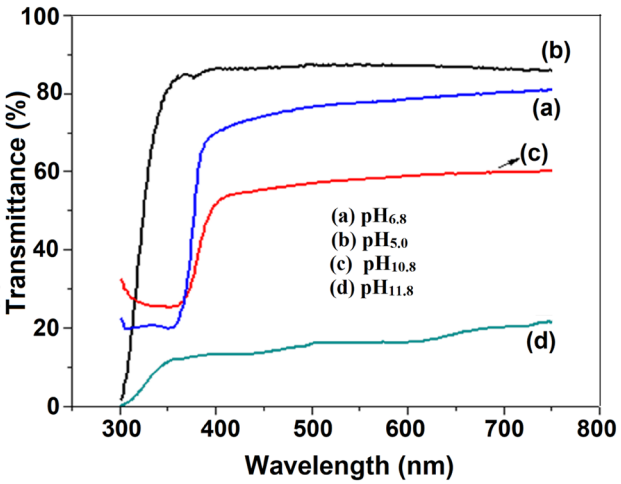

Fig. 2 Transmission spectra of as-grown ZnO thin films at various pH values

The absorption coefficient (α) was determined using transmittance curves. Figure 3 shows the variation of absorption coefficient with wavelength. It can be observed from the Fig. 3i, the absorption coefficient is constant in visible region for all the three samples. The values of absorption coefficient for $pH_{6.8}$, $pH_{5.0}$ and $pH_{10.8}$ were found to be 0.241×10^6/m, 0.170×10^6/m and 0.264×10^6/m at 500 nm, respectively. Lowest value of absorption coefficient in sample $pH_{5.0}$ indicated low absorption losses.

ZnO being a direct band-gap semiconductor, its optical band gap was obtained by extrapolating the corresponding straight line portions of the graphs between $(\alpha h\nu)^2$ versus the photon energy $h\nu$, till the intersection with energy axis. A blue shift in the band gap was observed in the sample $pH_{5.0}$ ($E_g = 4.01 \pm 0.009$ eV) as compared to the band gap of bulk ZnO (3.37 eV) at room temperature [38]. The increase in transmission and blue shift in absorption is due to the increase in grain sizes, structural homogeneity, and crystallinity of the sample $pH_{5.0}$ [40]. Blue shift in the absorption edge of $pH_{5.0}$ ZnO nanocrystalline films is related with the increase of the carrier concentration blocking the lowest states in the conduction band, well known as the Burstein–Moss effect [41]. Burstein pointed out that the lifting of the Fermi level into the conduction band of the degenerate semiconductor leads to the energy band broadening (blue shift) effect [42].The improved transmittance of $pH_{5.0}$ may also be attributed to its increased band gap and lesser thickness as compared to other samples.

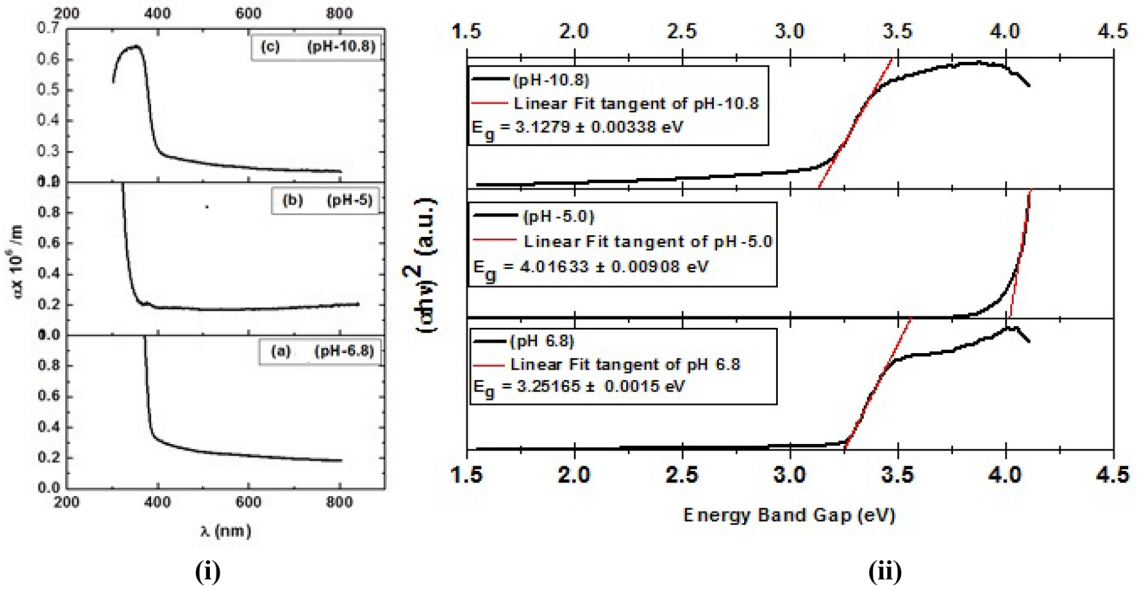

Fig. 3 **i** Absorption coefficients, **ii** band gaps of ZnO thin films at various pH values

From Fig. 4i, the reflectance values can be observed as 0.117, 0.071 and 0.184 at 500 nm, for the samples $pH_{6.8}$, $pH_{5.0}$ and $pH_{10.8}$, respectively. Hence, sample $pH_{5.0}$ showed minimum value of reflectance in the visible region which remained almost constant. Such result was expected because the same sample showed maximum transmittance among all the samples.

Using the reflectance data refractive index (n) of a material may be calculated using the following relation [43].

$$n = \frac{1 + R^{1/2}}{1 - R^{1/2}} \tag{18}$$

Figure 4ii reveals that refractive indices for $pH_{6.8}$, $pH_{5.0}$ and $pH_{10.8}$ are 2.05, 1.72 and 2.51, respectively at 500 nm. These values suggest that refractive index of thin film may be optimized by monitoring the pH of the precursor solution.

The dielectric constant of the deposited films was calculated using the following equation.

$$\varepsilon_{r=n^2-\kappa^2} \tag{19}$$

ε_r is the real part of dielectric constant and is a measure of how much it will slow down the speed of light in the material and κ is the imaginary part of dielectric constant and gives that how a dielectric absorbs energy from electric field due to dipole moment. It can be observed that $pH_{5.0}$ exhibited minimum dielectric constant as compared to that of $pH_{6.8}$ and $pH_{10.8}$. The values of ε_r as measured using the graph in Fig. 4iii were found to be 4.2, 2.95 and 6.29 respectively at 500 nm.

Refractive index and absorption coefficient, which are calculated using UV–Vis data, can also be used to calculate optical conductivity of a material using the following relation [44].

$$\sigma = \frac{nc\alpha}{4\pi} \tag{20}$$

Figure 4iv illustrates the variation of optical conductivity with wavelength. It was also observed to be affected by pH of the precursor solution. Figure 4iv showed the respective values of optical conductivity to be 0.11×10^{14}/s, 0.068×10^{14}/s and 0.157×10^{14}/s for $pH_{6.8}$, $pH_{5.0}$ and $pH_{10.8}$ at 500 nm. The sample $pH_{5.0}$ exhibited minimum and constant value of optical conductivity due to the low absorbance and low refractive index as compare to other samples.

Since the refractive index/dielectric constant both the quantities are directly related to the film thickness, as the film thickness of sample $pH_{5.0}$ is 802 nm. In comparison to other three samples this thickness is least, hence the value of refractive index and dielectric constant found minimum in sample $pH_{5.0}$. Such observations are well in agreement with the previously published reports [45, 46].

Figure 5 shows the FTIR spectra of thin films deposited at different pH values and concentrations. From Fig. 5i one can observed that the peaks at 430 cm^{-1} in $pH_{6.8}$, 435 cm^{-1} in $pH_{5.8}$ and 421 cm^{-1} in $pH_{10.8}$, were signature of Zn–O stretching vibrational modes in the deposited thin films. The vibration band of ZnO shifted from 435 to 421 cm^{-1} wave number with the change in pH. This shift may be caused due to the change in the morphology of ZnO with pH and also reported by Wahab et al. [47]. The symmetric stretching bands around 1336 cm^{-1} in $pH_{6.8}$ and 1356 cm^{-1} in $pH_{5.8}$ were assigned to NO_3^{-1} group and a weaker broad band

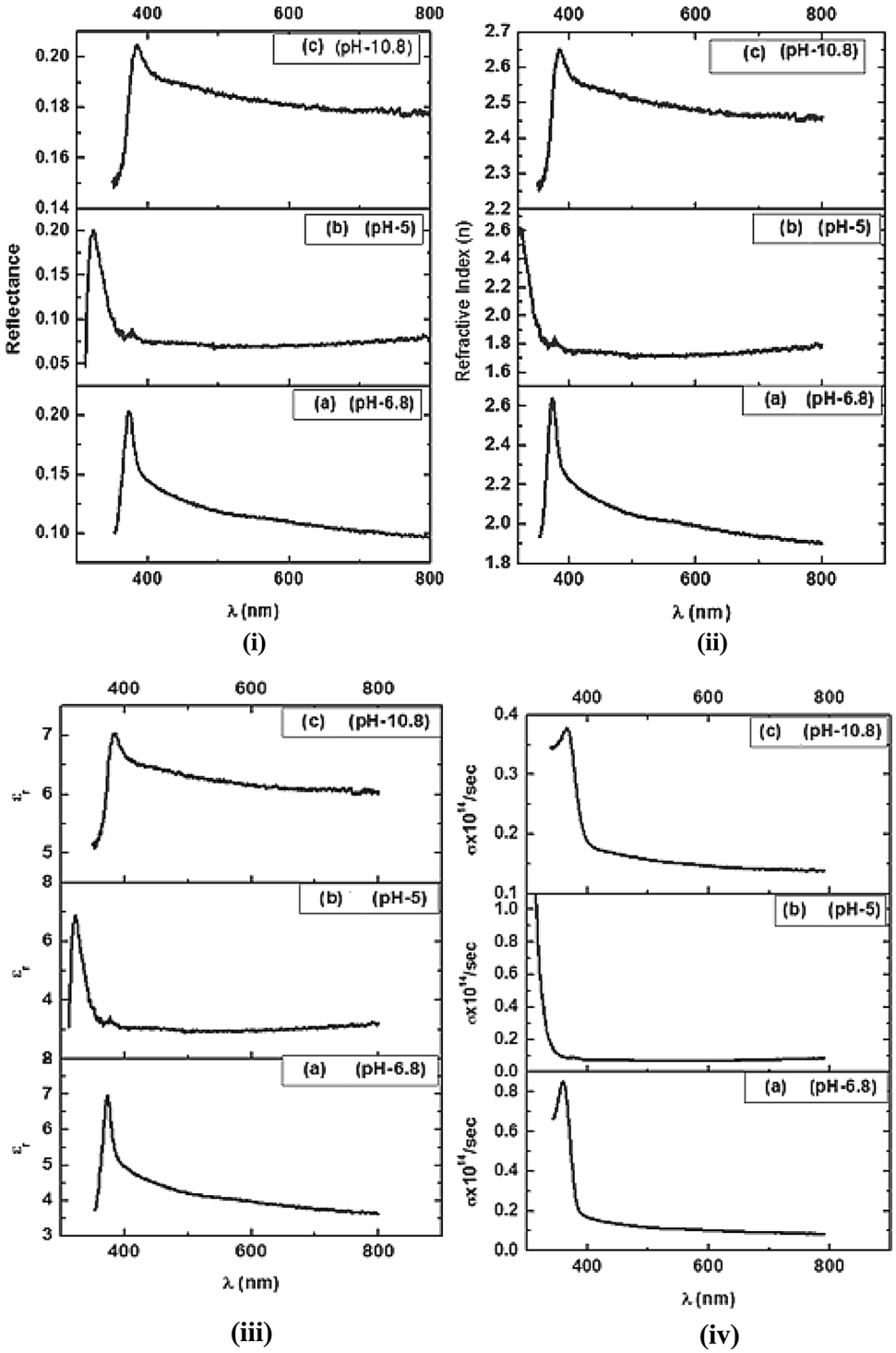

Fig. 4 **i** Reflectance, **ii** refractive index, **iii** dielectic constant and **iv** absorption coefficient of ZnO thin films at various pH values

in $pH_{6.8}$ around 3335 cm^{-1} could be assigned to the O–H stretching vibrations in H bonded water on the ZnO surface in sample $pH_{6.8}$ [45]. This band can be crosschecked through a weak 1635 cm^{-1} band due to scissor bending vibration of molecular water in $pH_{6.8}$. The weak peaks at 740 cm^{-1} and 891 cm^{-1} in $pH_{6.8}$ are due to the glass substrate, which was further confirmed by XRD. Figure 5ii shows the FTIR spectra of thin films deposited at various concentrations. It has been observed that sample fabricated using 100 mM concentration of both precursors was more pure as compared to the rest of the samples. Low Intensity bands in the finger print region could be attributed to the elements present in the glass substrates as observed in EDX spectra. The peak of Zn–O remained within the region 420 cm^{-1}

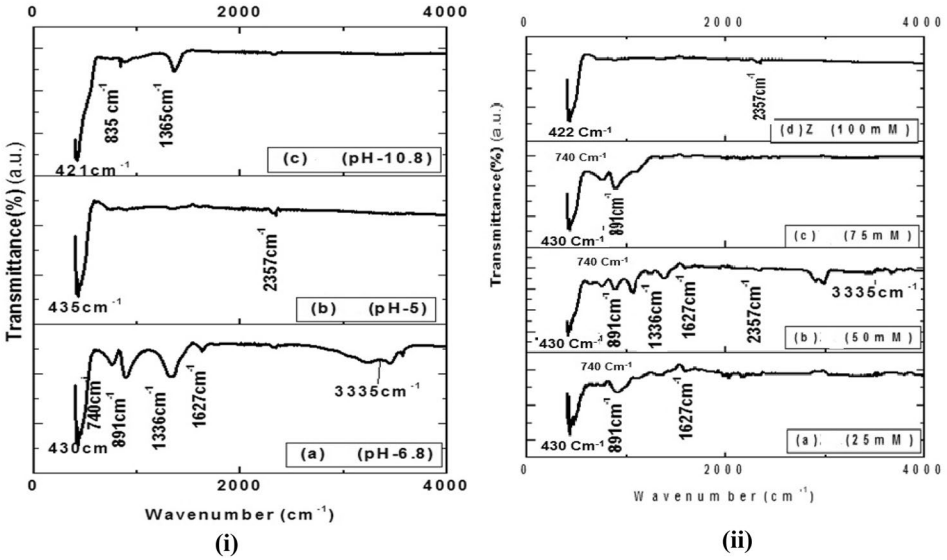

Fig. 5 FTIR of ZnO thin films at various **i** pH values, **ii** concentrations

to 440 cm^{-1}. The weak peak at 2330 cm^{-1} in the sample M_{100} was assigned to iso-nitrile group and the weak band at 2936 cm^{-1} in sample M_{50} was due to the C–H stretching of aldehyde group [48]. On the basis of extent of material coverage on the substrate, 100 mM was optimized for the further experiments.

3.4 Surface morphology and elemental analysis

Figure 6 shows the change in morphology of the nanostructures deposited at the glass substrate due to the change in pH value and concentration in bath. It was observed that particles showed highly dense flower like structures with two dimensional nanosheet petals perpendicular to the substrate at pH 6.8 (Fig. 6a). This vertical growth is attributed to the inherent anisotropy of the wurtzite (hcp) lattice structure of ZnO with an axial c/a ratio of 1.602 [49]. At pH 5.0, twinned rod morphologies aligned along the substrate were observed (Fig. 6b). Boyle et al. [19] reported that ZnO thin films using CBD process containing HMTA and a zinc salt at acidic pH 5.0, is a kinetically-controlled reaction involving relatively high concentrations of one, i.e., Zn^{2+} over the other i.e. OH^- component and slow precipitation of ZnO from $Zn(OH)_2$ encourages formation of branched nanorods aligned along the substrate.

At moderate pH environment, HMTA hydrolysis decreases leading to increase in pH value and assist initiation of secondary nucleate branches on nanorods side surface with advanced growth [34]. The change in rods shape from hexagonal ($pH_{5.0}$) to prism like shape ($pH_{6.8}$) was expected due to the electrostatic interaction between the ionic solution and ZnO polar faces and as a consequence higher miller indices became preferred. ZnO growth in basic bath $pH_{10.8}$ reveals flower type morphology with stars like petals (Fig. 6c). This structural growth may be attributed to exceeding amount of OH^- ions present in the bath at the basic pH due to the addition of NaOH and OH^- released from the fast hydrolysis of HMTA.

On varying the pH to basic side, concentration of Zn^{2+} ions is reduced as compared to OH^- ions. This corresponds to the reaction mechanism proposed by XU [50].

$$Zn^{2+} + 2OH^- \rightarrow Zn(OH)_2 \tag{21}$$

$$Zn(OH)_2 + H_2O \rightarrow Zn(OH)_4^{2-} \tag{22}$$

Eventually, $Zn(OH)_4^{2-}$ ions may lead to the formation of larger zinc hydroxide complexes which would ultimately precipitated into ZnO [51]. When the precipitation exceeds the number of nuclei, multi-angular orientation building blocks grow on the substrates and a three dimensional growth from the limited number of nuclei along their axes generates star-like flower structures as reported by Vayssieres [52].

Elemental phase compositions of deposited films were examined by energy dispersive X-ray spectroscopy (EDX). EDX system was integrated to SEM where the electron beam excites characteristic X-rays from the probed area. Figure 6a–c illustrate the chemical composition of the thin films corresponding to the pH value of 6.8, 5.0 and 10.8 respectively. The EDX spectra of these samples confirmed the purity of these films, which is manifested by the absence of impurity. Only a small peak of silica from the substrate or gold (Au) peak due to the gold coating of sample was observed.

Figure 7 shows the change in morphology of the nanostructures deposited at the glass substrate due to the change in concentration. SEM studies revealed that the morphology of as grown particles of the thin film is closely related with

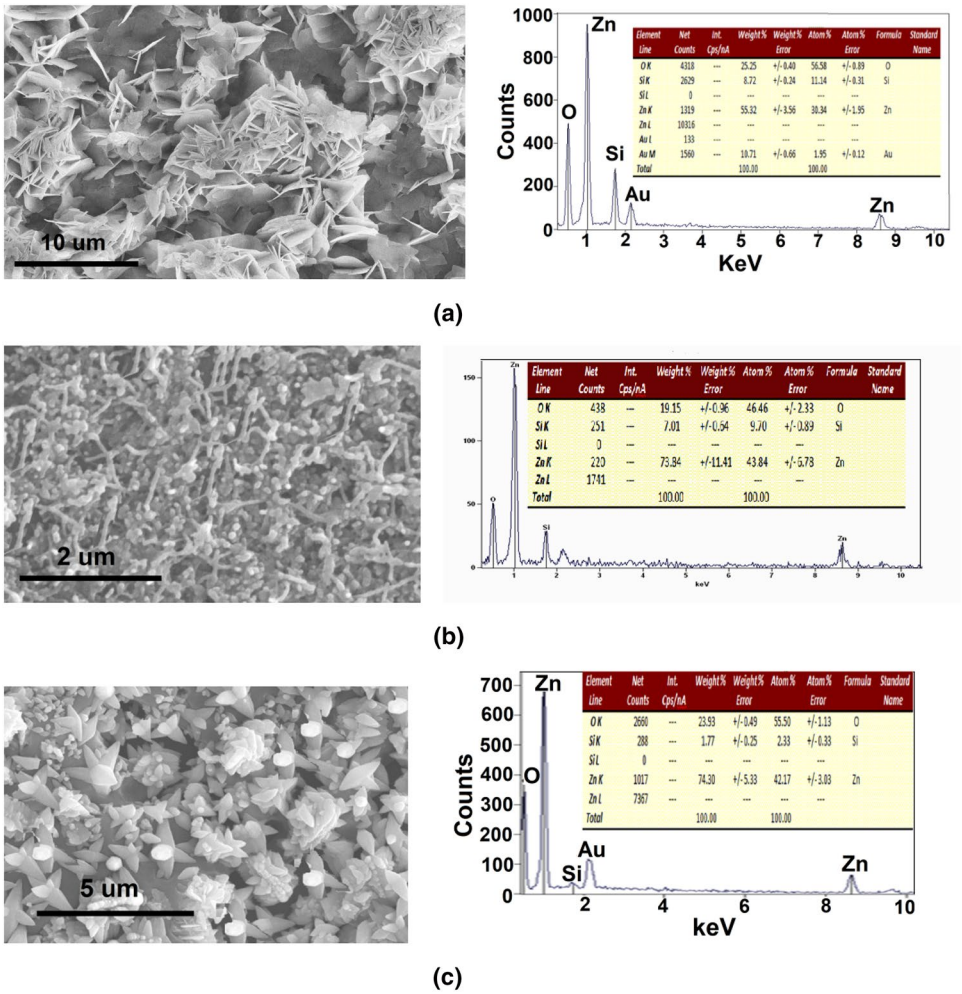

Fig. 6 SEM images of ZnO thin films at **a** $pH_{6.8}$, **b** $pH_{5.0}$ and **c** $pH_{10.8}$

the precursor concentration. SEM micrograph (Fig. 7a) of sample M_{25} exhibited agglomerates of ZnO nano-crystals. Whereas sample M_{50} (Fig. 7b) prepared with 50 mM concentration exhibited highly dense and oriented nano-walls, perpendicular to the substrate which is due to the fact that the nucleation density on the substrate increased as the zinc concentration in the solute increased. As the solution concentration exceeded 50 mM, the average diameter of the particles increased due to the clustering of nano-walls, which reversed the orientation and as a result sample M_{75} (75 mM) shows growth of a few rods (Fig. 7c) along the substrate. However, the samples under high precursor (sample M_{100}) concentration were dense but with poor degree of orientation (Fig. 7d). In general with increasing zinc concentration in the bath, zinc potential is raised. The rise in the chemical potential of zinc in the chemical solution is compensated by the generation of more nucleation sites on the substrate and as a result highly branched structural growth is enhanced in sample M_{100}. SEM micrographs for all the samples were compared to observe the substrate coverage and it was concluded that only sample M_{100} could nearly cover the whole substrate. The presence of Zn and O was confirmed by corresponding EDX peaks. The presence of an intense peak of silica along with small peaks of Ca, Al and K in the EDX spectra corresponding to M_{25}, M_{50} and M_{75} (Fig. 7a–c) suggested incomplete coverage of the substrates. The EDX spectra of Fig. 7d reflect the purity of M_{100} as compared to the rest of the samples, as intensity of silica peak is very small as compared to zinc and no other impurity peak is visible in it. Nearly complete coverage of the substrate in M_{100} along with high purity of the zinc oxide nano thin films suggested that M_{100} sample can be chosen for the further electrical studies. Au peak is from gold coating of the sample. It has been observed that the zinc content in the films increase with the increase in the concentration and the films consist of Zinc and oxygen only.

3.5 Sheet resistance

Finally, sheet resistance of the thin film deposited at different pH values at a fixed molar concentration of 100 mM for both the precursors was measured using Keithley source

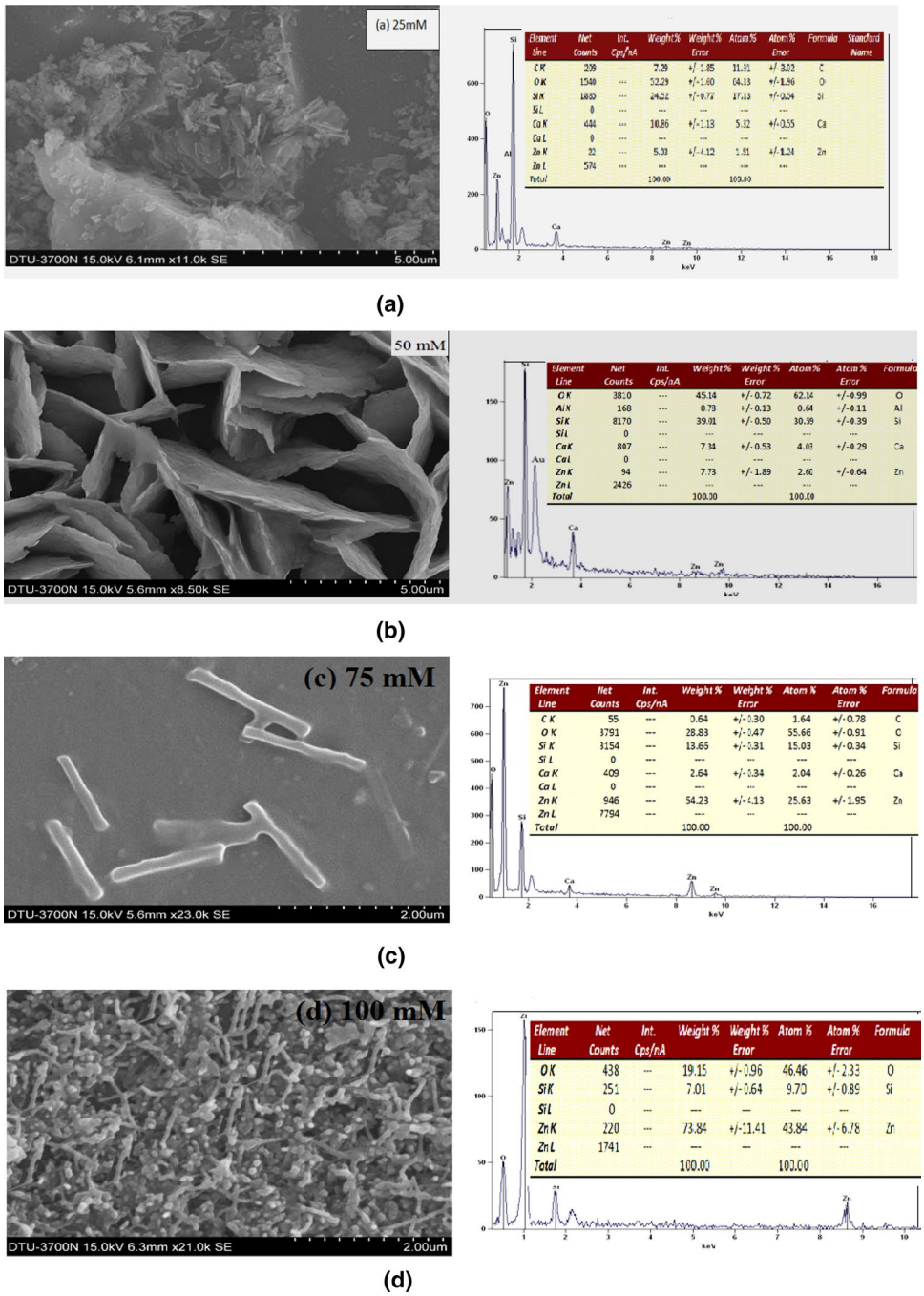

Fig. 7 SEM images of ZnO thin films at **a** 25 mM, **b** 50 mM, **c** 75 mM and **d** 100 mM

meter (model-2450). This instrument can source and measure both current and voltage and can be configured to display resistance and resistivity. Sheet resistance for $pH_{6.8}$ was 8.75×10^5 Ω/square, for $pH_{5.0}$ it was 6.8×10^8 Ω/square and for $pH_{10.8}$ -1.33×10^5 Ω/square. High resistance transparent buffer layer at pH 5.0 can also improve solar cell efficiencies by reducing the necessary thickness of the buffer layer and by reducing the shorting through the buffer layer. On the basis of maximum transmittance and sheet resistance, lowest absorption coefficient and refractive index exhibited by sample at pH 5.0 and due the highest band gap among the three samples ($pH_{6.8}$, $pH_{5.0}$ and $pH_{10.8}$) deposited at different pH, was selected finally as the best buffer layer sample for thin film solar cell application.

4 Conclusion

ZnO thin films were successfully fabricated on seeded glass slides using chemical bath deposition technique by firstly varying pH values and then by variable precursor concentrations. pH and concentration variation studies finally shows that nearly complete coverage of the substrate along with high purity of the zinc oxide thin films is observed at pH 5.0 and at equal 100 mM concentration of $Zn(NO_3)$ and HMTA. So it was concluded that the samples fabricated at pH 5.0 using 100 mM concentration for both precursors can be used as a buffer layer in thin film solar cell as it shows improved band gap 4.0 eV, high transmittance (87%), low absorption coefficient 0.170×10^6/m, low reflectance (0.071), low refractive index (1.72), low dielectric constant 2.95 and low optical conductivity $(0.068 \times 10^{14}$/s) at 500 nm incident radiation. The thin film synthesized at pH 5.0 also exhibited highest value of sheet resistance which is very important for high solar cell efficiency. The results presented in this study demonstrated that both the pH as well as the precursor concentration of the chemical bath solution has strong influence on the optical, structural and morphological properties of ZnO thin films.

Acknowledgements This work was partially supported by the National Research Foundation of Korea (NRF) vide Korea government (MSIP) Nos. 2016R1A6A1A03012877, 2018R1D1A1B07051095 and 2018R1D1A1B07050237. Authors from MM University, Mullana are also thankful to the Department of Science and Technology (DST), New Delhi, India for supporting the part of this research work (vide Project No. SR/FTP/PS-69/2008), dated 15/1/2010. One of the Authors, Ravi Kant Choubey is thankful to the Council of Science & Technology, Lucknow, Uttar Pradesh, India for the financial support (Vide No. CST/4051).

References

1. X. Wang, C.J. Summers, Z.L. Wang, Nano Lett. **4**, 423 (2004)
2. T.W. Hamann, A.B.F. Martinson, J.W. Elam, M.J. Pellin, J.T. Hupp, Adv. Mater. **20**, 1560 (2008)
3. H. Meruvu, M. Vangalapati, S.C. Chippada, S.R. Bammidi, Rasayan J. Chem. **4**, 217 (2011)
4. N. Jones, B. Ray, K.T. Ranjit, A.C. Manna, FEMS Microbiol. Lett. **279**, 71 (2008)
5. X. Liu, X. Wu, H. Cao, R.P.H. Chang, J. Appl. Phys. **95**, 3141 (2004)
6. O. Lupan, L. Chow, G. Chai, L. Chernyak, O.L. Tirpak, H. Heinrich, Phys. Status Solidi A **205**, 2673 (2008)
7. L. Saad, M. Riad, J. Serb. Chem. Soc. **73**, 997 (2008)
8. J.A. Nikolaev, V.J. Rud', J.V. Rud', FTP 36 No 9, 1128 (2002). (In Russian)
9. D. Hariskos, S. Spiering, M. Powalla, Thin Solid Films **480–481**, 99 (2005)
10. A.K. Radzimska, T. Jesionowski, Materials **7**, 2833 (2014)
11. Z. Fan, J.G. Lu, J. Nanosci. Nanotechnol. **5**, 1561 (2005)
12. L. Vayssieres, K. Keis, S.E. Lindquist, A. Hagfeldt, J. Phys. Chem. B **105**, 3350 (2001)
13. B.D. Yao, Y.F. Chan, N. Wang, Appl. Phys. Lett. **81**, 757 (2002)
14. H. Yuan, Y. Zhang, J. Cryst. Growth **263**, 119 (2004)
15. Y. Sun, G.M. Fuge, M.N.R. Ashfold, Chem. Phys. Lett. **396**, 21 (2004)
16. Y.W. Heo, V. Varadarajan, M. Kaufman, K. Kim, D.P. Norton, F. Ren, P.H. Fleming, Appl. Phys. Lett. **81**, 3046 (2002)
17. W.T. Chiou, W.Y. Wu, J.M. Ting, Diam. Relat. Mater. **12**, 1841 (2003)
18. D. Lin, H. Wu, W. Pan, Adv. Mater. **19**, 3968 (2007)
19. D.S. Boyle, K. Govender, P. O'Brien, Chem. Commun. **1**, 80 (2002)
20. C.C. Lin, H.P. Chen, S.Y. Chen, Chem. Phys. Lett. **404**, 30 (2005)
21. D. Vernardou, G. Kenanakis, S. Couris, E. Koudoumas, E. Kymakis, N. Katsarakis, Thin Solid Films **515**, 8764 (2007)
22. D. Polsongkram, P. Chamninok, S. Pukird, O. Lupan, Physica B **403**, 3713 (2008)
23. R.K. Choubey, D. Desai, S.N. Kale, S. Kumar, J. Mater. Sci.: Mater. Electron. **27**, 7890 (2016)
24. R.K. Choubey, S. Kumar, C.W. Lan, Adv. Nat. Sci.: Nanosci. Nanotechnol. **5**, 025015 (2014)
25. Y.S. Lo, R.K. Choubey, W.C. Yu, W.T. Hsu, C.W. Lan, Thin Solid Films **520**, 217 (2011)
26. P. O'Brien, J. McAleese, J. Mater. Chem. **8**, 2309 (1998)
27. G. Hodes, *Chemical Solution Deposition of Semiconductor Film* (Dekker, New York, 2002)
28. W.T. Hsu, S.S. Ro, H.R. Hsu, Y.C. Liu, Thin Solid Films **529**, 293 (2013)
29. D. Byrne, E.M.C. Glyn, J. Cullin, M.O. Henry, Nanoscale **3**, 1675 (2011)
30. K. Govender, S.B. David, P.B. Kenway, P. O'Brien, J. Mater. Chem. **14**, 2575 (2004)
31. S. Xu, L.W. Zhong, Nano Res. **4**, 1013 (2011)
32. M.O. Lopez, A. Avila-Garcia, M.L. Albor-Aguilera, V.M. Sanchez-Resendiz, Mater. Res. Bull. **38**, 1241 (2003)
33. H. Tada, J. Am. Chem. Soc. **82**, 255 (1960)
34. T.A. Vijayan, R. Chandramohan, S. Valanarasu, J. Thirumalai, S. Venkateswaran, T. Mahalingam, S.R. Srikumar, Sci. Technol. Adv. Mater. **9**, 035007 (2008)
35. G.R. Patil, R.S. Gaikwad, M.B. Shelar, R.S. Mane, S.H. Han, B.N. Pawar, Arch. Phys. Res. **3**, 401 (2012)
36. M. Shaban, M. Zayed, H. Hamdy, R. Soc. Chem. **7**, 617 (2017)
37. K.V. Gurav, U.M. Patil, S.M. Pawar, J.H. Kim, C.D. Lokhande, J. Alloys Compd. **509**, 7723 (2011)
38. A. Janotti, C.G. Van de Walle, Rep. Prog. Phys. **72**, 126501 (2009)
39. E. Muchuweni, T.S. Sathiaraj, H. Nyakotyo, Heliyon **3**, e00285 (2017)
40. K. Nadarajah, C.Y. Chee, C.Y. Tan, J. Nanomater. (2013). https://doi.org/10.1155/2013/146382
41. E. Burstein, Phys. Rev. **93**, 632 (1954)
42. E. Burstein, Phys. Rev. **25**, 7826 (1982)
43. D.D.O. Eya, A.J. Ekpunobi, C.E. Okeke, Pac. J. Sci. Technol. **6**, 16 (2005)
44. P. Sharma, A. Dahshan, K.A. Aly, J. Alloys Compd. **616**, 323 (2014)
45. S. Sharma, C. Periasamy, P. Chakrabarti, Electron. Mater. Lett. **11**, 1093 (2015)
46. P.B. Taunk, R. Das, D.P. Bisen, R.K. Tamrakar, N. Rathor, Karbala Int. J. Mod. Sci. **1**, 159 (2015)
47. R. Wahab, Y.S. Kim, H.S. Shin, Mater. Trans. **50**, 2092 (2009)
48. G.M. Lampman, D.L. Pavia, G.S. Kriz, J.R. Vyvyan, *Spectroscopy*, 4th edn. (Cengage Learning India, New Delhi, 2010), p. 56
49. A. Sugunan, C.W. Hemant, M. Boman, J. Dutta, J. Sol-Gel Sci. Technol. **39**, 49 (2006)

50. S. Xu, Semiconductor Nanomaterials for Flexible Technologies. 2010; 197
51. W.J. Li, E.W. Shi, W.Z. Zhong, Z.W. Yin, J. Cryst. Growth **203**, 186 (1999)
52. L. Vayssieres, Adv. Semicond. Nanostruct. C. R. Chim. **9**, 691 (2006)